PROCEEDINGS OF SCIENCE

Machine Learning Analysis for Dark Matter Detection via Photon Signatures at the LHC

Rosa María Sandá Seoane[a,b,*]

[a] *Departamento de Física Teórica, Universidad Autónoma de Madrid, C/ Francisco Tomás y Valiente 7, Campus de Cantoblanco, 28049, Madrid, Spain*
[b] *Instituto de Física Teórica UAM-CSIC, C/ Nicolás Cabrera 13-15, Campus de Cantoblanco, 28049, Madrid, Spain*

E-mail: rosa.sanda@uam.es

The search for weakly interacting massive particles (WIMPs) remains a central goal of the High Luminosity Large Hadron Collider (HL-LHC). In this work, we explore radiative neutralino decays within the framework of the Z_3-symmetric Next-to-Minimal Supersymmetric Standard Model (NSSM), focusing on scenarios where the lightest supersymmetric particle (LSP) is a singlino-dominated neutralino. In this setting, the correct dark matter relic density can be achieved through coannihilation with higgsino- or bino-like states, while also evading current direct detection bounds via blind spot conditions. In particular, in singlino–higgsino coannihilation scenarios, radiative decays of the heavier neutralinos into the singlino LSP and a photon can be significantly enhanced, motivating dedicated searches at the HL-LHC. These decays yield challenging final states characterized by at least one soft photon, a lepton, and a large missing transverse energy signature, enhanced by a hard initial-state radiation jet. We employ a Machine Learning (ML)–based analysis that enhances sensitivity to these faint signatures, providing a robust, data-driven complement to conventional search strategies in the exploration of new physics scenarios. Our results demonstrate that the use of ML classifiers significantly improves the discrimination power against Standard Model (SM) backgrounds, offering promising discovery potential in this well-motivated dark matter (DM) scenario.

The European Physical Society Conference on High Energy Physics (EPS-HEP2025)
7-11 July 2025
Marseille, France

[*]Speaker

© Copyright owned by the author(s) under the terms of the Creative Commons Attribution-NonCommercial-NoDerivatives 4.0 International License (CC BY-NC-ND 4.0) All rights for text and data mining, AI training, and similar technologies for commercial purposes, are reserved. ISSN 1824-8039 . Published by SISSA Medialab.

PoS(EPS-HEP2025)440

1. Introduction

The discovery of the Higgs boson confirmed the mechanism of electroweak symmetry breaking and completed the SM spectrum. Nevertheless, the SM leaves open fundamental questions, such as the nature of DM and the stability of the electroweak scale. Low-scale supersymmetry [1–3] provides a well-motivated extension, offering a stable LSP as a DM candidate, when R-parity is conserved, protecting the Higgs mass from large quantum corrections, and addressing other theoretical shortcomings of the SM.

In this study, we focus on a compressed electroweakino spectrum in the Z_3-symmetric NMSSM [4], where the LSP ($\tilde{\chi}_1^0$) is singlino-dominated, i.e., originated from the singlet sector, while the next-to-lightest states $\tilde{\chi}_2^0$ and $\tilde{\chi}_1^\pm$ are higgsino-like. Such LSP is a viable WIMP-like DM candidate (since it is electrically neutral, stable, and weakly interacting), but requires efficient annihilation to satisfy relic density constraints. The NMSSM offers different possibilities to account for this, but our analysis concentrates on the so-called "compressed region" of the parameter space, where the relic density arises predominantly from co-annihilation between a singlino-like LSP and nearly degenerate higgsino states (assuming also that sleptons are heavy and decoupled).

Direct detection experiments have reached impressive sensitivity, placing strong bounds on DM–nucleon interactions mediated by the Higgs and Z bosons. Singlino-like DM at the electroweak scale can remain viable in "blind spot" regions, where the relevant couplings are suppressed [5, 6]. Recently, Ref. [7] derived novel blind spot conditions for singlino-like DM that emerges through mixing effects with bino and higgsino states,

$$\left(m_{\tilde{\chi}_1^0} + \frac{g_1^2 v^2}{M_1 - m_{\tilde{\chi}_1^0}}\right) \frac{1}{\mu_{\text{eff}} \sin 2\beta} \simeq 1 \,. \tag{1}$$

Thus, the blind spot condition essentially depends on the relative sign between μ_{eff} and M_1, requiring them to be opposite for $\kappa > 0$, and the same sign if $\kappa < 0$. These results enlarge the parameter space consistent with direct detection limits, rendering collider searches in the compressed spectra particularly complementary.

In the considered regime, we focus on the region of the parameter space where loop-induced radiative decays of both higgsino-like states $\tilde{\chi}_2^0$ and $\tilde{\chi}_3^0$ become dominant ($\tilde{\chi}_2^0 \to \tilde{\chi}_1^0\gamma$ and $\tilde{\chi}_3^0 \to \tilde{\chi}_2^0\gamma$), yielding photon-rich final states that provide distinctive collider signatures, largely unexplored by standard LHC searches optimized for wino-like electroweakinos.

To probe these challenging compressed scenarios, we employ ML techniques to enhance LHC sensitivity in events with soft photons in the final state, thereby enabling the HL-LHC to access regions of parameter space that remain inaccessible to traditional cut-and-count strategies, as already shown in [8] in an analogous final state within the MSSM. We consider proton-proton collisions at $\sqrt{s} = 14$ TeV with 100 fb^{-1}, focusing on higgsino-like $\tilde{\chi}_3^0\tilde{\chi}_1^\pm/\tilde{\chi}_2^0\tilde{\chi}_1^\pm$ pair-production in association with a hard ISR jet to boost the system and improve missing transverse energy signature (E_T^{miss}) signatures. Using both binned-likelihood [9](BL) and unbinned ML-based likelihood approaches (the latter relies on the Machine-Learned Likelihood (MLL) method introduced in [10, 11]), we demonstrate that this novel photon-rich channel could significantly extend the discovery potential for elusive DM candidates at the LHC, even in regions beyond the reach of current and future direct

PoS(EPS-HEP2025)440

detection experiments. Further details on the results presented in this proceeding can be found in the associated work [12].

2. Setup

As outlined in Section 1, the signal under study arises from two distinct processes, illustrated in Figure 1. We study radiatively decaying neutralinos at $\sqrt{s} = 14$ TeV, requiring a hard ISR jet in association with higgsino-like $\tilde{\chi}_1^\pm \tilde{\chi}_2^0$ or $\tilde{\chi}_1^\pm \tilde{\chi}_3^0$ production,

$$p\,p \to \tilde{\chi}_1^\pm \tilde{\chi}_2^0\, j / \tilde{\chi}_1^\pm \tilde{\chi}_3^0\, j, \;\; \tilde{\chi}_1^\pm \to \tilde{\chi}_1^0 \ell \nu_\ell, \;\; \tilde{\chi}_3^0 \to \tilde{\chi}_2^0 + \gamma, \;\; \tilde{\chi}_2^0 \to \tilde{\chi}_1^0 + \gamma.$$

Signal and background generation and event selection. Signal events were generated with MadGraph5_aMC@NLO [13]+Pythia8 [14]+Delphes [15], using the NMSSM UFO implementation, and spanning benchmark points with $m_{\tilde{\chi}_2^0} \in [150, 290]$ GeV and $m_{\tilde{\chi}_2^0} - m_{\tilde{\chi}_1^0} \in [3, 30]$ GeV. The selected benchmark points (BPs) are representative of the compressed region, with only a limited subset yielding the correct cosmological relic density. Details about the model and the theoretical and experimental constraints applied to the BPs can be found in [12]. Backgrounds include W+jets, $W\gamma$, $t\bar{t}$+jets. Subdominant contributions from processes such as Z+jets, single-top, $t\bar{t}\gamma$, and diboson production are also taken into account, while all other sources were found to be negligible. Event selection requires at least one lepton, at least one photon, at least one jet with $p_T > 100$ GeV, and $E_T^{\text{miss}} > 100$ GeV. Object identification criteria are based on the standard ATLAS Run 2 optimized selections, consistent with detector performance guidelines.

Machine learning implementation. For the analysis of the simulated data, we follow the strategy first proposed in [8]. At its core, this approach employs the `XGBoost` [16] algorithm, a gradient-boosted decision tree classifier widely adopted in high-energy physics (also in several ATLAS and CMS searches) due to its robustness in handling complex, high-dimensional datasets and its regularization mechanisms that mitigate overfitting.

For training, we generate 200k signal and 200k background events, ensuring balanced datasets, while assigning equal statistics to each BP and properly weighting the background contributions. While merging all BPs into a single dataset may not be fully optimal for individual points, it provides a general classifier applicable across the parameter space without retraining. An independent test sample, constructed analogously, is used to assess the final performance of the trained model.

In order to train the classifier, we considered a comprehensive set of kinematic variables describing the final-state topology. The low-level features include the transverse momentum and pseudorapidity of the leading jet ($p_T^{j_1}$, η^{j_1}), lepton ($p_T^{\ell_1}$, η^{ℓ_1}), and photon ($p_T^{\gamma_1}$, η^{γ_1}), as well as the missing transverse energy (E_T^{miss}), and the multiplicities of jets (n_j), leptons (n_ℓ), and photons (n_γ). To further enhance the signal-to-background discrimination, we complemented these with high-level observables such as the total hadronic activity (H_T^{jets}), the global transverse energy (H_T), the transverse masses of the leading jet ($m_T^{j_1}$), lepton ($m_T^{\ell_1}$), and photon ($m_T^{\gamma_1}$), the scalar sum of the leading objects (s_T^1), and the missing-energy significance ($E_T^{\text{miss}}/\sqrt{H_T}$). Together, these variables provide a balanced representation of both detector-level information and derived observables, forming the complete input feature set for the supervised binary classifier.

Significance Estimation. Although the classifier input is high-dimensional, its one-dimensional output represents the probability of an event being signal and can be used to compute exclusion

PoS(EPS-HEP2025)440

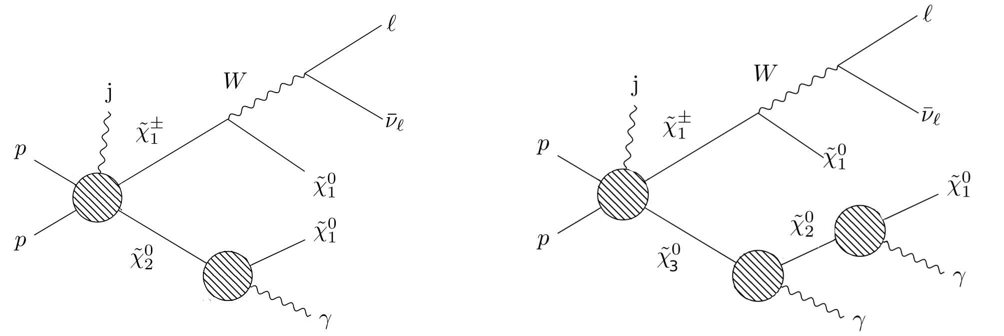

Figure 1: Feynman diagrams illustrating the two production modes of higgsino-like states. Left: $pp \rightarrow \tilde{\chi}_2^0 \tilde{\chi}_1^\pm j$. Rigth: $pp \rightarrow \tilde{\chi}_3^0 \tilde{\chi}_1^\pm j$.

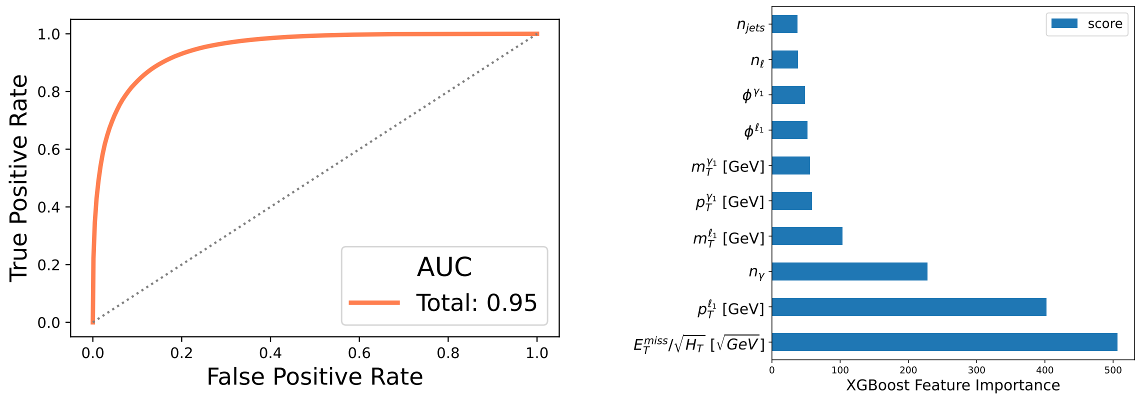

Figure 2: Left: ROC curve and corresponding AUC value for the XGBoost classifier. Right: feature importance ranking (gain metric).

($Z = 2$) and discovery ($Z = 5$) significances like any other discriminating variable. We employ two complementary approaches to perform this statistical inference: the Binned Likelihood (BL) method and the Machine-Learned Likelihood (MLL) technique. In the BL approach, the classifier output is discretized into a histogram. The expected numbers of signal and background events in each bin are used to construct a Poisson-based likelihood, which is then employed to define the log-likelihood ratio test statistic and estimate the significance (Z_{BL}). While widely used, this method can incur a loss of information due to the binning procedure, potentially smearing subtle features in the classifier distribution. By contrast, the MLL method avoids binning by performing an unbinned fit. In this case, the likelihood combines a global Poisson term for the total number of events with event-by-event probability density functions (PDFs) for signal and background, encoding the event-by-event information. Kernel Density Estimators (KDEs) are employed to approximate these PDFs using the classifier outputs. The resulting unbinned likelihood allows a more precise evaluation of the log-likelihood ratio and the expected discovery significance Z_{MLL}, which is estimated numerically through pseudo-experiments with signal-plus-background events. The formulae for statistical treatment can be found in [10, 11]. Results displayed in next section only include statistical uncertainties. A sketch of the possible inclusion on systematic uncertainties within the MLL method can be found in [8, 17].

PoS(EPS-HEP2025)440

3. Results

In this section, we present the main results of the analysis. The performance of the binary classifier is illustrated in Figure 2, where the left panel shows the ROC curve and the area under the curve (AUC = 0.95), indicating excellent discrimination between signal and background. The right panel displays the ten most relevant features according to the gain metric, with missing transverse energy significance, leading lepton kinematics, and photon characteristics being the most important.

Figure 3 shows the one-dimensional distributions of the six most discriminant features for two representative benchmark points: BP1-3 with low neutralino masses and BP9-3 with higher masses. The missing transverse energy significance ($E_T^{\rm miss}/\sqrt{H_T}$) is the most powerful variable, reflecting the presence of undetected neutralinos in the signal, while the leading lepton transverse momentum ($p_T^{\ell_1}$) is softer than in the SM due to off-shell W decays in the compressed spectrum. The number of photons (n_γ) highlights the relevance of the $\tilde{\chi}_1^\pm \tilde{\chi}_3^0$ production channel, which produces more photons through a longer decay chain.

Figure 4 shows the projected LHC sensitivity for compressed electroweakinos. Using 100 fb^{-1} at 14 TeV, we achieve a 5σ discovery for $m_{\tilde{\chi}_2^0} \lesssim 225$ GeV with mass splittings $\lesssim 12$ GeV, and 2σ exclusion up to 285 GeV for splittings $\lesssim 20$ GeV. Sensitivity increases for smaller splittings due to enhanced photon branching ratios but decreases below ~ 7 GeV when photons become too soft. The channel $pp \to \tilde{\chi}_1^\pm \tilde{\chi}_3^0$ compensates in the ultra-compressed region, and boosted neutralino-chargino systems allow detection even below the nominal photon p_T threshold. Current LHC limits, derived with `CheckMate` [18], exclude up to $m_{\tilde{\chi}_2^0} \sim 140$ GeV for intermediate mass splittings, while our proposed signal extends coverage to ~ 280 GeV.

Direct detection constraints, rescaled by the neutralino relic density, are satisfied for all benchmark points due to near blind-spot conditions ($M_1 \simeq 500$ GeV). The neutrino floor limits the sensitivity of future direct detection experiments, yet the LHC can probe scenarios with cross sections below this floor for splittings up to 20 GeV and $m_{\tilde{\chi}_2^0} \sim 170$ GeV. This demonstrates the complementarity of collider searches and direct detection in exploring dark matter candidates inaccessible to current experiments, highlighting the importance of the proposed novel signal channel. The full set of results and its analysis can be found in [12].

4. Conclusions

We have investigated a novel search strategy for neutralinos in the Z_3–symmetric NMSSM, focusing on compressed spectra where the singlino-like LSP ($\tilde{\chi}_1^0$) is nearly degenerate with higgsino-like states ($\tilde{\chi}_2^0$, $\tilde{\chi}_3^0$, and $\tilde{\chi}_1^\pm$). In this regime, traditional hadronic, dilepton, and trilepton searches lose sensitivity due to suppressed branching ratios, while radiative decays into photons become dominant. We thus explored final states with one or two soft photons plus a hard ISR jet, a channel not previously studied at the LHC. Importantly, this region of parameter space coincides with novel blind spots of direct detection proposed in [7], where the DM–nucleus cross section is suppressed, highlighting the complementarity of collider searches.

To overcome the challenges posed by low cross-sections and soft signatures, we implemented ML-based analyses that exploit correlations among kinematic variables, surpassing the reach of conventional cut-based approaches. Our projections at the HL-LHC, that can be found in [12] with

PoS(EPS-HEP2025)440

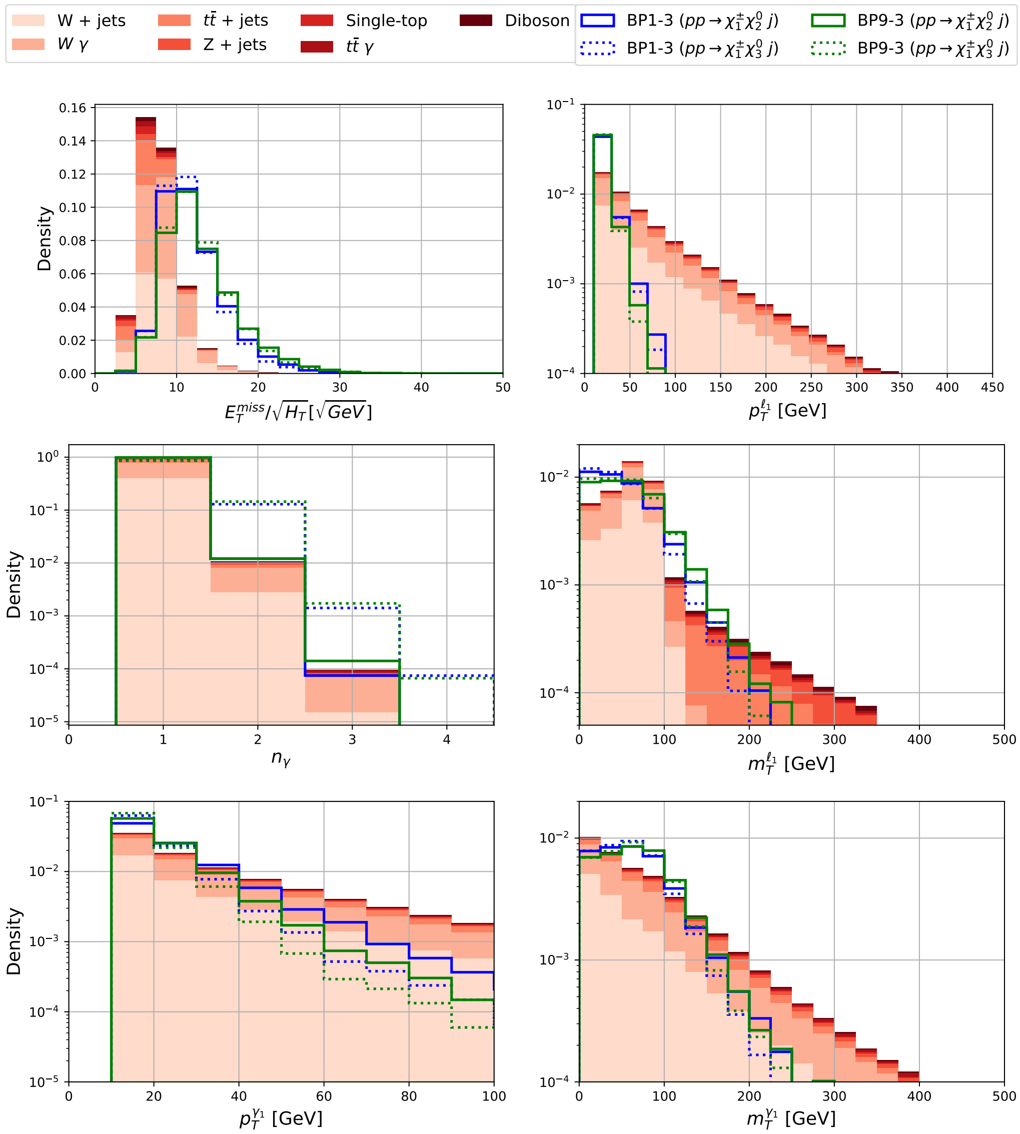

Figure 3: Distributions of the six final-state kinematic observables with the highest discriminating power between signal and background: missing transverse energy significance ($E_T^{\text{miss}}/\sqrt{H_T}$); transverse momentum of the leading lepton ($p_T^{\ell_1}$); photon multiplicity (n_γ); transverse mass of the leading lepton ($m_T^{\ell_1}$); transverse momentum of the leading photon ($p_T^{\gamma_1}$); and transverse mass of the leading photon ($m_T^{\gamma_1}$). Two benchmark scenarios are shown: BP1-3 with lighter masses ($\tilde{\chi}^0_{1,2,3} \sim$ 145–165 GeV) and BP9-3 with heavier masses ($\tilde{\chi}^0_{1,2,3} \sim$ 235–250 GeV). The production modes are presented separately: $pp \to \tilde{\chi}_1^\pm \tilde{\chi}_2^0 j$ (solid lines) and $pp \to \tilde{\chi}_1^\pm \tilde{\chi}_3^0 j$ (dotted lines).

PoS(EPS-HEP2025)440

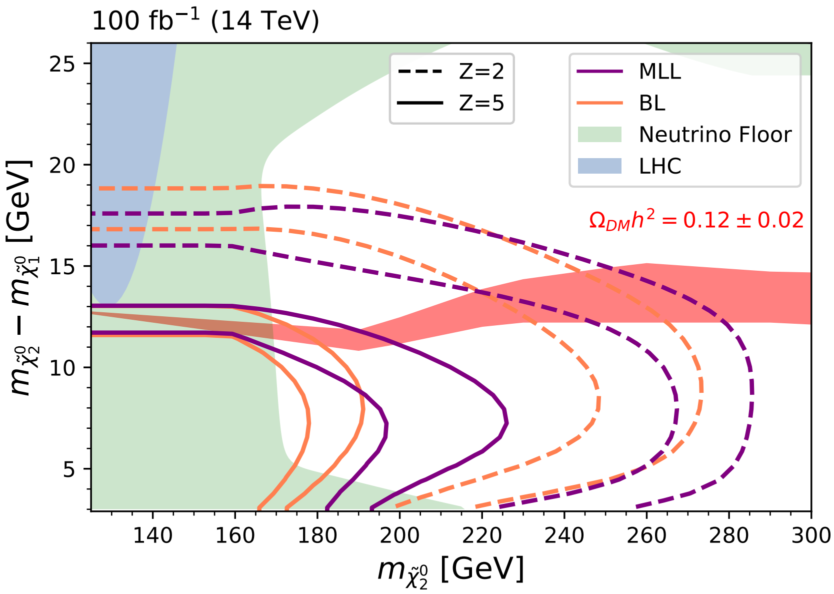

Figure 4: Contours of the projected discovery significance in the $[m_{\tilde{\chi}_2^0}, m_{\tilde{\chi}_2^0} - m_{\tilde{\chi}_1^0}]$ plane: $Z = 2$ (dashed) and $Z = 5$ (solid). Results are shown for the BL strategy (orange) and for the MLL approach (violet).

the full set of results, show promising discovery and exclusion sensitivities, comparable to previous results in the MSSM case [8], and capable of probing scenarios inaccessible to direct detection experiments. These results motivate a dedicated effort by experimental collaborations, including refined treatments of systematic uncertainties, to fully exploit this complementary search channel for dark matter with photon signatures at the HL-LHC.

Acknowledgements

R.M.S.S. was supported by the Ramón y Cajal Fellowship contract RYC-2017-22986, and acknowledge partial financial support by the Spanish Research Agency (Agencia Estatal de Investigación) through the grants CNS2023-144536, PID2021-124704NB-I00, and IFT Centro de Excelencia Severo Ochoa No CEX2020-001007-S, funded by MCIN/AEI/10.13039/501100011033.

References

[1] H. P. Nilles, Phys. Rept. **110**, 1-162 (1984) doi:10.1016/0370-1573(84)90008-5

[2] H. E. Haber and G. L. Kane, Phys. Rept. **117**, 75-263 (1985) doi:10.1016/0370-1573(85)90051-1

[3] S. P. Martin, Adv. Ser. Direct. High Energy Phys. **18**, 1-98 (1998) doi:10.1142/9789812839657_0001 [arXiv:hep-ph/9709356 [hep-ph]].

[4] U. Ellwanger, C. Hugonie and A. M. Teixeira, Phys. Rept. **496**, 1-77 (2010) doi:10.1016/j.physrep.2010.07.001 [arXiv:0910.1785 [hep-ph]].

PoS(EPS-HEP2025)440

[5] M. Badziak, M. Olechowski and P. Szczerbiak, JHEP **03**, 179 (2016) doi:10.1007/JHEP03(2016)179 [arXiv:1512.02472 [hep-ph]].

[6] S. Baum, M. Carena, N. R. Shah and C. E. M. Wagner, JHEP **04**, 069 (2018) doi:10.1007/JHEP04(2018)069 [arXiv:1712.09873 [hep-ph]].

[7] S. Roy and C. E. M. Wagner, JHEP **04**, 106 (2024) doi:10.1007/JHEP04(2024)106 [arXiv:2401.08917 [hep-ph]].

[8] E. Arganda, M. Carena, M. de los Rios, A. D. Perez, D. Rocha, R. M. Sandá Seoane and C. E. M. Wagner, JHEP **07**, 014 (2025) doi:10.1007/JHEP07(2025)014 [arXiv:2410.13799 [hep-ph]].

[9] G. Cowan, K. Cranmer, E. Gross and O. Vitells, Eur. Phys. J. C **71**, 1554 (2011) [erratum: Eur. Phys. J. C **73**, 2501 (2013)] doi:10.1140/epjc/s10052-011-1554-0 [arXiv:1007.1727 [physics.data-an]].

[10] E. Arganda, M. de los Rios, A. D. Perez and R. M. Sandá Seoane, PoS **ICHEP2022**, 1226 (2022) doi:10.22323/1.414.1226

[11] E. Arganda, A. D. Perez, M. de los Rios and R. M. Sandá Seoane, Eur. Phys. J. C **83**, no.12, 1158 (2023) doi:10.1140/epjc/s10052-023-12314-z [arXiv:2211.04806 [hep-ph]].

[12] E. Arganda, M. de los Rios, A. D. Perez, S. Roy, R. M. Sandá Seoane and C. E. M. Wagner, [arXiv:2509.15121 [hep-ph]].

[13] J. Alwall, R. Frederix, S. Frixione, V. Hirschi, F. Maltoni, O. Mattelaer, H. S. Shao, T. Stelzer, P. Torrielli and M. Zaro, JHEP **07**, 079 (2014) doi:10.1007/JHEP07(2014)079 [arXiv:1405.0301 [hep-ph]].

[14] T. Sjöstrand, S. Ask, J. R. Christiansen, R. Corke, N. Desai, P. Ilten, S. Mrenna, S. Prestel, C. O. Rasmussen and P. Z. Skands, Comput. Phys. Commun. **191**, 159-177 (2015) doi:10.1016/j.cpc.2015.01.024 [arXiv:1410.3012 [hep-ph]].

[15] J. de Favereau *et al.* [DELPHES 3], JHEP **02**, 057 (2014) doi:10.1007/JHEP02(2014)057 [arXiv:1307.6346 [hep-ex]].

[16] T. Chen and C. Guestrin, doi:10.1145/2939672.2939785 [arXiv:1603.02754 [cs.LG]].

[17] E. Arganda, D. A. Díaz, A. D. Perez, R. M. Sandá Seoane and A. Szynkman, Phys. Rev. D **109**, no.5, 055032 (2024) doi:10.1103/PhysRevD.109.055032 [arXiv:2309.05407 [hep-ph]].

[18] D. Dercks, N. Desai, J. S. Kim, K. Rolbiecki, J. Tattersall and T. Weber, Comput. Phys. Commun. **221**, 383-418 (2017) doi:10.1016/j.cpc.2017.08.021 [arXiv:1611.09856 [hep-ph]].

PoS(EPS-HEP2025)440